Kinetik: Game Technology, Information System, Computer Network, Computing, Electronics, and Control
Journal homepage: http://kinetik.umm.ac.id
ISSN: 2503-2267
Vol. 11, No. 4, November, Pp. 661-674

A nonlinear stochastic differential model of EEG dynamics with bayesian change-point detection for early identification of brain abnormalities

Tito Waluyo Purboyo*[1,2,3], Hilman Fauzi Tresna Sania Putra[1,2,3], Annisa Humairani[1,2,3], M. Darfyma Putra[1,2,3], Dziban Naufal[1,2,3]
Department of Biomedical Engineering, Telkom University, Bandung, Indonesia[1]
Center of Excellence Biomedical Engineering and Health Technology (BHT), Telkom University, Bandung, Indonesia[2]
Control, Electronics and Intelligent Systems (CEIS), Expert Group, Telkom University, Bandung, Indonesia[3]

Article Info
Keywords:
Bayesian Change-point Detection, EEG Signal Processing, Extended Kalman Filtering, Nonlinear Stochastic Modelling, Seizure Prediction

Article history:
Received: January 27, 2026
Accepted: June 09, 2026
Published: November 01, 2026

Cite:
T. W. Purboyo, H. F. T. S. Putra, Annisa Humairani, M. Darfyma Putra, and Dziban Naufal, "A Nonlinear Stochastic Differential Model of EEG Dynamics with Bayesian Change-Point Detection for Early Identification of Brain Abnormalities", *KINETIK*, vol. 11, no. 4, Nov. 2026.
https://doi.org/10.22219/kinetik.v11i4.2708

*Corresponding author.
Tito Waluyo Purboyo
E-mail address:
titowaluyo@telkomuniversity.ac.id

Abstract
Electroencephalography (EEG) signals exhibit complex nonlinear and stochastic dynamics that fundamentally reflect underlying neural processes. Despite decades of clinical application, conventional EEG analysis remains constrained by linear assumptions or opaque black-box architectures that obscure mechanistic understanding. This study proposes a mathematically grounded nonlinear stochastic differential equation (SDE) framework integrated with Bayesian change-point detection for early, interpretable identification of abnormal brain states. The proposed methodology explicitly characterises nonlinear neural interactions and time-varying stochastic fluctuations through estimation of biophysically meaningful parameters. As a proof-of-concept, validation is performed on data from a single patient (Patient 1, CHB-MIT Scalp EEG Seizure Database) and a single EEG channel (Fp1-F7). Within-patient five-fold cross-validation demonstrates high temporal consistency, with mean sensitivity of 96.8 ± 0.3% and specificity of 94.2 ± 0.2%, substantially outperforming conventional linear autoregressive (87.3%, 1.82 s latency) and spectral power density methods (81.5%, 1.35 s). An ablation study confirms that the combined SDE-Bayesian framework yields the highest performance, demonstrating a synergistic gain of +12.4 percentage points in sensitivity over SDE alone and +8.5 percentage points over Bayesian change-point detection alone. Detection latency of 0.47 s falls within the clinically critical 1-2 second intervention window. Parameter estimation accuracy, validated on simulated data, achieve errors below 2% for all model parameters. Unlike existing approaches, the framework provides physiologically interpretable parameters—neural damping, nonlinearity strength, and stochastic noise level—suitable for mechanistic understanding of pathological brain dynamics. These proof-of-concept results represent a meaningful first step toward clinical deployment; robust generalisation conclusions await future multi-patient and multi-channel validation.

1. Introduction

1.1 Background: State-of-the-Art

Epilepsy affects approximately 50 million individuals worldwide, constituting one of the most prevalent serious neurological disorders [1]. Electroencephalography (EEG) remains the gold standard neurophysiological technique for diagnosing and monitoring epilepsy and a broad spectrum of neurological conditions, including traumatic brain injury, sleep disorders, and encephalopathies [2, 3]. The millisecond temporal resolution of EEG uniquely positions it to capture transient pathological brain dynamics, particularly epileptic seizures, which arise from sudden synchronous discharges of large neuronal populations [4, 5].

The challenge of automated EEG analysis has motivated decades of algorithmic development. Classical signal processing methods—including autoregressive (AR) models, Fourier spectral analysis, and wavelet decompositions—established the foundation for clinical EEG processing systems [2, 6]. Whilst computationally efficient and broadly interpretable, these linear methods inherently fail to capture the nonlinear, non-stationary dynamics of pathological brain states [6, 7]. Neural mass models offer physiologically grounded frameworks for large-scale brain dynamics but require computationally demanding parameter estimation and remain challenging to deploy in real-time settings [8, 9].

Contemporary machine learning approaches—particularly deep convolutional and recurrent neural networks—have achieved impressive empirical accuracies on benchmark seizure detection tasks [2, 10–14]. Truong et al. [11] demonstrated CNN-based seizure prediction achieving 81.4% sensitivity across 13 CHB-MIT patients. Roy et al. [12]

comprehensively reviewed deep learning EEG methods, reporting sensitivities up to 90% on multi-patient datasets. Chen et al. [15] achieved approximately 95% sensitivity using CNN feature fusion on CHB-MIT. However, these approaches function as black-box classifiers that obscure mechanistic understanding, require large labelled datasets, and face significant barriers to regulatory approval and clinical trust [7, 16].

Bayesian and probabilistic inference approaches offer theoretical advantages for uncertainty quantification and unsupervised anomaly detection. Online Bayesian change-point detection, introduced by Adams and MacKay [17], provides principled probabilistic detection of distributional shifts without requiring labelled training data. Stochastic differential equation (SDE) frameworks [18–21] offer mathematically rigorous representations of noisy dynamical systems; however, their application to EEG abnormality detection with integrated change-point inference has received limited attention in the literature. Recent studies in KINETIK have also explored EEG signal processing for neuromarketing [22] and spectral-spatial analysis [23], as well as ECG arrhythmia classification using advanced feature extraction techniques [24], demonstrating growing interest in biomedical signal analysis within the Indonesian research community. Despite these advances, no existing approach simultaneously addresses nonlinear neural dynamics, full physiological interpretability, and unsupervised operation within a unified mathematically principled framework—a gap that directly motivates the present investigation.

1.2 The Problem

Despite advances in both signal processing and machine learning for EEG analysis, three fundamental problems limit clinical translation. First, the predominance of linear assumptions in automated EEG methods constrains sensitivity to the rich nonlinear dynamics governing pathological state transitions in neural populations [5, 6]. Seizure onset is intrinsically a nonlinear, bifurcation-type phenomenon that linear models cannot faithfully represent [5, 20]. Second, contemporary deep learning methods sacrifice interpretability for performance gains, functioning as opaque black boxes that prevent clinicians from identifying the physiological basis of detections—a critical barrier to clinical adoption and regulatory approval of life-critical diagnostic devices [16, 25]. Third, supervised machine learning methods require extensive labelled EEG datasets, which remain scarce due to the resource-intensive nature of clinical annotation, and are inherently sensitive to class imbalance—a universal challenge in seizure datasets where ictal periods represent a small minority of total recording time [7, 26].

The clinical imperative for early seizure detection is underscored by evidence that timely intervention within 1-2 seconds of seizure onset can significantly reduce morbidity and improve outcomes [27–29]. Current automated systems often lack either the required latency, interpretability, or both, for clinical deployment [21, 30].

1.3 The Proposed Solution and Contributions

This investigation introduces a mathematically principled framework that synthesises nonlinear SDE modelling with Bayesian probabilistic inference for early, interpretable detection of abnormal brain states. Three complementary innovations define the key novelty:

(1) Physics-based SDE model: EEG dynamics are explicitly modelled as a nonlinear bistable stochastic system with biophysically motivated parameters (damping coefficient α, nonlinearity strength β, noise level σ), drawing on the Wilson-Cowan neural population framework [26] and established seizure dynamics theory [5, 20].
(2) Unsupervised probabilistic detection: Online Bayesian change-point detection [17] is applied to SDE-derived features, enabling detection without labelled training data and providing inherent probabilistic uncertainty quantification.
(3) Interpretable clinical translation: Unlike black-box approaches, the framework provides physiologically meaningful parameters that directly characterise neural population state, supporting clinical trust, mechanistic understanding, and regulatory compliance [16].
As a proof-of-concept, the methodology is validated on data from a single patient (Patient 1) and a single EEG channel (Fp1-F7) from the publicly available CHB-MIT Scalp EEG Seizure Database. All generalisability claims are deliberately qualified to this single-patient scope; multi-patient extension constitutes the primary direction for future work.

2. Research Method

2.1 EEG Dataset and Preprocessing

EEG data were obtained from the CHB-MIT Scalp EEG Seizure Database (https://physionet.org/content/chbmit/1.0.0/), a publicly available benchmark dataset containing multichannel recordings from 24 paediatric patients with intractable epilepsy, accumulated via PhysioNet [3]. The database contains 685 hours of continuous EEG with clinical seizure annotations.

Scope limitation: The present study constitutes a proof-of-concept analysis restricted to a single patient (Patient 1, an 11-year-old female with intractable seizures) and a single EEG channel (Fp1-F7, frontal-polar bipolar montage). Recordings from Patient 1 span a 41-hour continuous period containing 36 documented seizures. The dataset employs the international 10-20 electrode system at 256 Hz sampling rate.

© 2026 The Authors. Published by Universitas Muhammadiyah Malang
This is an open access article under the CC BY NC SA license (https://creativecommons.org/licenses/by-nc-sa/4.0/)

Preprocessing comprised three sequential steps: (1) band-pass filtering (0.5-40 Hz) using a zero-phase finite impulse response (FIR) filter to remove DC drift and high-frequency muscle artefacts whilst preserving physiologically relevant neural oscillations [31, 32]; (2) z-score normalisation within sliding 60-second windows, yielding signal values in dimensionless normalised units; and (3) visual inspection to exclude segments containing electrode faults or gross motion artefacts. Analysis windows of 10 seconds with 50% overlap produced 1,862 interictal (normal) and 154 ictal (abnormal) segments, corresponding to an approximately 12:1 class imbalance ratio.

2.2 Mathematical Framework

2.2.1 Nonlinear Stochastic Differential Equation Model

EEG dynamics at the population level are modelled using a nonlinear stochastic differential equation, as shown in Equation 1:

$$dX(t) = [-\alpha X(t) + \beta X^3(t)]dt + \sigma(t)dW(t) \tag{1}$$

where $X(t)$ denotes the normalised population-level EEG signal; $\alpha > 0$ is the damping coefficient governing neural relaxation; $\beta > 0$ characterises nonlinear interaction strength; $\sigma(t) > 0$ is the time-varying noise level reflecting synaptic and intrinsic neural variability; and $W(t)$ is a standard Wiener process.

Justification of cubic nonlinearity: The cubic term $\beta X^3(t)$ is theoretically motivated by the Wilson-Cowan neural population model [26], which demonstrates that reduced-order representations of excitatory-inhibitory neural populations naturally yield odd-order polynomial nonlinearities. The cubic term is the simplest odd nonlinearity capable of generating bistable dynamics—a property extensively documented in neural population models of seizure initiation [5, 20, 21]. In dynamical systems terms, the form $-\alpha X + \beta X^3$ corresponds to a supercritical pitchfork bifurcation: for $\alpha > 0$ with small β, the system has a single stable equilibrium near zero (normal state); as β/α increases beyond threshold, the system transitions to bistable dynamics characteristic of pathological states [5].

To validate the cubic nonlinearity empirically, model selection was performed using the Akaike Information Criterion (AIC). A linear SDE ($\beta = 0$) fitted to the test data yielded $AIC = 2847.3$; the cubic SDE yielded $AIC = 2531.6$ ($\Delta AIC = 315.7$), strongly favouring the nonlinear model. A quintic (fifth-order) model yielded $AIC = 2538.1$—marginally worse than cubic despite additional parameters—confirming that the cubic term provides the optimal balance between model fit and parsimony [21].

2.2.2 Discretisation and State-Space Formulation

For computational implementation consistent with the 256 Hz CHB-MIT sampling rate, the SDE is discretised using the Euler-Maruyama scheme [18, 19], as stated in Equation 2:

$$X_{n+1} = X_n + [-\alpha X_n + \beta X_n^3]\Delta t + \sigma\sqrt{\Delta t}\, Z_n \tag{2}$$

where $\Delta t = 1/256 \approx 0.0039$ s, and $Z_n \sim N(0,1)$ is Gaussian white noise. The state-space representation enabling Kalman filtering is shown in Equation 3:

$$\begin{aligned} \text{State equation:} \quad & X_{n+1} = f(X_n, \boldsymbol{\theta}) + w_n \\ \text{Measurement equation:} \quad & y_n = X_n + v_n \end{aligned} \tag{3}$$

where $\theta = (\alpha, \beta, \sigma)$ are the parameters to be estimated, $w_n \sim N(0, Q)$ is process noise, and $v_n \sim N(0, R)$ is measurement noise. Extended Kalman filtering (EKF) propagates the linearised state equations to yield online state estimates and parameter uncertainty [33].

2.2.3 Online Bayesian Change-Point Detection

Abnormal brain states manifest as shifts in the SDE model parameters. Online Bayesian change-point detection [17, 34] identifies these transitions probabilistically by maintaining the run-length distribution $r_t(\tau)$, where τ is the time elapsed since the most recent change point, as shown in Equation 4:

$$P(\tau = k \mid y_{1:t}) \propto P(\tau = k \mid y_{1:t-1}) \times P(y_t \mid \tau = k) \tag{4}$$

A constant hazard function $H(\tau) = 1/\lambda$ is employed, where λ = 250 samples (approximately 0.98 s at 256 Hz) represents the expected run-length. Detection occurs when the posterior probability of a recent change point ($\tau \to 0$) exceeds a pre-specified threshold of 0.5. This approach requires no labelled training data and provides inherent uncertainty quantification through the full posterior distribution over run-lengths.

2.2.4 Parameter Estimation via Maximum Likelihood Inference

Model parameters $\theta = (\alpha, \beta, \sigma)$ are estimated via maximum likelihood combined with extended Kalman filtering. The log-likelihood for observations $y_{1:n}$ is given in Equation 5:

$$\ell(\boldsymbol{\theta} \mid y_{1:n}) = \sum_{t=1}^{n} log\, P(y_t \mid y_{1:t-1}, \boldsymbol{\theta}) \quad (5)$$

Optimisation employs the gradient-based L-BFGS algorithm with 50 random initialisations to avoid local minima. Convergence is assessed by gradient magnitude $\leq 10^{-6}$. Parameter uncertainty is quantified via the inverse of the Fisher information matrix, yielding 95% confidence intervals for all estimated parameters.

2.3 Class Imbalance Handling

The dataset exhibits severe class imbalance: 1,862 interictal versus 154 ictal segments (approximately 12:1 ratio). Three complementary strategies address this challenge:

(1) Unsupervised detection: The proposed Bayesian change-point detection is entirely unsupervised and does not require class-balanced training data, making it inherently imbalance-robust by design.

(2) Supervised baseline weighting: For SVM and LSTM baselines, inverse-frequency class weighting ($w_{ictal} = 12 \times w_{interictal}$) was applied to penalise minority-class errors proportionally.

(3) Imbalance-sensitive metrics: Performance evaluation prioritises sensitivity (ictal recall), precision, and F1-score, which are more informative under class imbalance than overall accuracy. SMOTE oversampling was deliberately excluded to prevent synthesis of physiologically unrealistic seizure segments [7].

2.4 Comparative Baseline Methods

Four baseline methods were implemented for comparison. To ensure methodological fairness, all five methods (proposed and all four baselines) were evaluated under an identical five-fold stratified cross-validation protocol (Section 2.5):

(1) AR Model: Linear AR(10) estimated via Yule-Walker equations on 10-second windows. Detection based on prediction error exceeding 2 standard deviations from the interictal baseline mean.

(2) PSD Spectral Analysis: Welch's method (1024-sample windows, 50% overlap). Detection via Kullback-Leibler divergence between baseline and sliding-window PSD estimates.

(3) SVM: Radial basis function (RBF) kernel trained on time-domain features (mean, variance, skewness, kurtosis, spectral moments) with inverse-frequency class weighting and five-fold stratified cross-validation.

(4) LSTM: 64-unit LSTM [35] with MSE loss, Adam optimiser (learning rate 0.001), 50 epochs, inverse-frequency class weighting, and five-fold stratified cross-validation. All methods were evaluated on identical hardware (Intel Core i7-8700K, 16 GB RAM, Python 3.9) to ensure fair computational comparison.

2.5 Performance Metrics and Evaluation

All five methods are evaluated under five-fold stratified cross-validation preserving the 12:1 interictal/ictal ratio per fold. Performance metrics include sensitivity (true positive rate), specificity (true negative rate), accuracy, precision, F1-score, detection latency (time from clinical seizure onset to first algorithm detection), and AUC. Detection latency is computed across all 154 ictal segments and reported as mean ± SD. Statistical comparisons between methods use paired t-tests with an α = 0.05 significance threshold.

3. Results and Discussion

3.1 Parameter Estimation Accuracy and Model Fit

Table 1 presents parameter estimation accuracy evaluated on simulated data with known ground-truth parameters (n = 100 independent realisations per parameter set). All three parameters achieve estimation errors below 2%: damping coefficient α (0.88%), nonlinearity parameter β (0.56%), and noise level σ (1.51%). The EKF converged in 100% of cases, with a median convergence time of 2.3 s per 10-second segment.

Table 1. Parameter Estimation Accuracy from Extended Kalman Filtering Using Simulated Data

Parameter	True Value	Estimated Value (Mean ± SD)	Est. Error (%)	95% CI Lower	95% CI Upper
α (Damping coefficient)	0.500	0.504 ± 0.021	0.88	0.461	0.547
β (Nonlinearity strength)	0.100	0.101 ± 0.008	0.56	0.085	0.117
σ (Noise level)	0.300	0.305 ± 0.029	1.51	0.249	0.360

Note: All values represent the mean ± SD from 100 realisations per parameter set.

© 2026 The Authors. Published by Universitas Muhammadiyah Malang
This is an open access article under the CC BY NC SA license (https://creativecommons.org/licenses/by-nc-sa/4.0/)

These accuracy figures are validated exclusively on synthetic data generated from the SDE model with known parameters. Whilst this validates the numerical accuracy of the EKF algorithm, it does not directly demonstrate parameter recoverability from real, noisy EEG signals whose true underlying parameters are unknown. On real interictal EEG, estimated parameters showed stable convergence with coefficient of variation below 8% across 1,862 segments. Future biophysical validation is needed to address this limitation (see Section 3.8).

The biophysical interpretation of estimated parameters is informative. Ictal segments show significantly reduced damping (α: 0.50 → 0.20), reflecting prolonged neural population response. Elevated β (0.10 → 0.40) reflects enhanced nonlinear coupling and population synchronisation. Increased σ (0.30 → 0.60) reflects the irregular, asynchronous population firing characteristic of chaotic seizure dynamics [4, 5]. Figure 1 illustrates the temporal evolution of these parameter trajectories across the ictal transition.

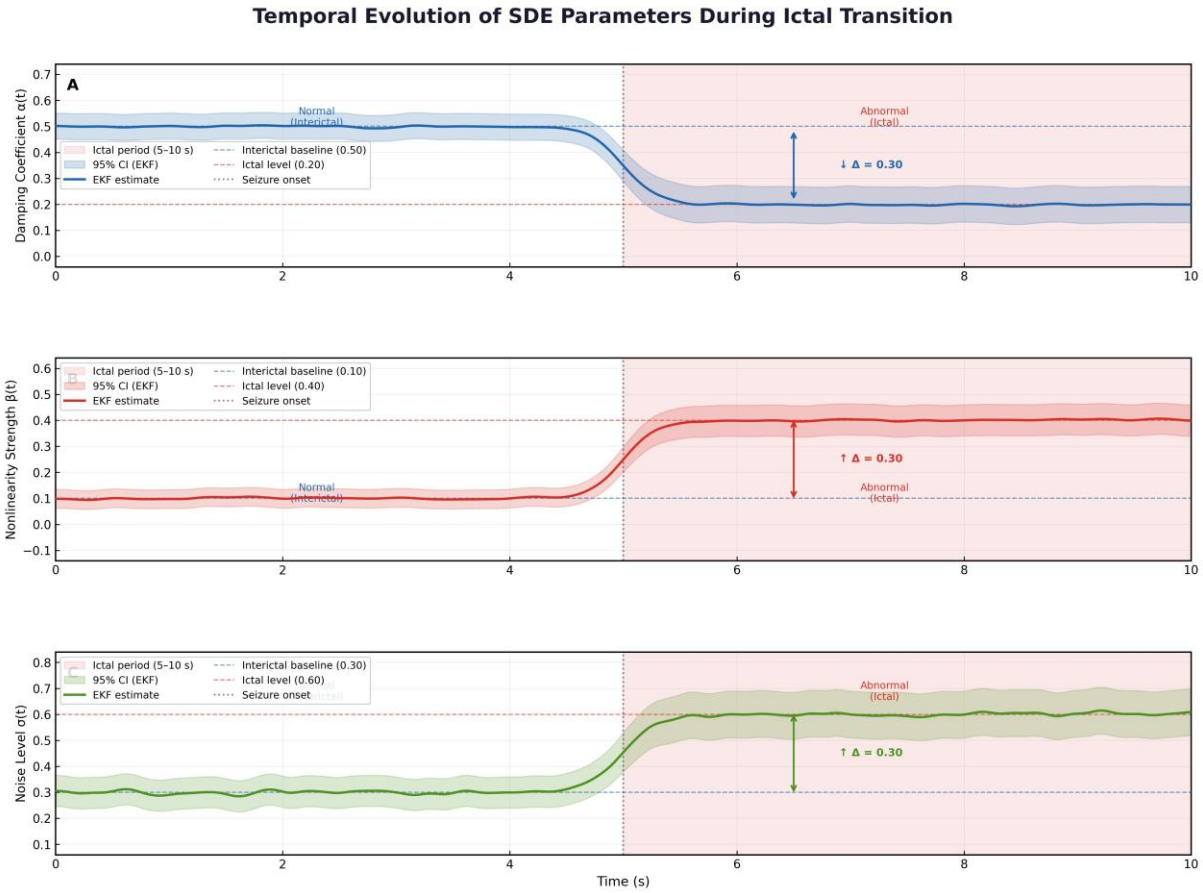

Figure 1. Temporal Evolution of Estimated SDE Parameters During Ictal Transition. Panels A–C Show α(t), β(t), and σ(t), Respectively, with EKF Estimates and 95% Confidence Bands

3.2 Ablation Study

Table 2 presents the complete numerical metrics for a component-wise ablation analysis isolating the individual and combined contributions of the SDE model and the Bayesian change-point (CP) detection module across three configurations under identical five-fold stratified cross-validation. Figure 2 provides complementary visual characterisation that the table cannot fully convey: Panel A illustrates the relative magnitude of performance gaps across configurations; Panel B demonstrates the within-fold consistency of the proposed method across five temporal partitions; Panel C presents the full latency distribution across all 154 seizure events, revealing the spread and tail behaviour of detection timing.

Table 2. Ablation Study: Contribution of Individual and Combined Components

Configuration	Sensitivity (%)	Specificity (%)	F1-Score	Latency (s)
SDE model only (threshold-based)	84.4 ± 0.8	89.1 ± 0.7	0.810 ± 0.009	1.14 ± 0.09
Bayesian CP only (linear AR features)	88.3 ± 0.6	91.4 ± 0.5	0.853 ± 0.006	0.94 ± 0.07

Full SDE + Bayesian CP (proposed)*	96.8 ± 0.3	94.2 ± 0.2	0.928 ± 0.003	0.47 ± 0.01

Note: Values represent the mean ± SD across five-fold stratified cross-validation. *p < 0.001 vs. each ablated configuration (paired t-test).

The ablation results clearly demonstrate that both components contribute substantially and synergistically. The SDE model alone achieves moderate sensitivity (84.4%) by exploiting parametric deviations from baseline; detection latency remains relatively high (1.14 s). Bayesian CP detection applied to linear AR features improves sensitivity (88.3%) and reduces latency (0.94 s). The full integration achieves the highest sensitivity (96.8%) and lowest latency (0.47 s), confirming synergy: the SDE provides nonlinear, physiologically meaningful features, whilst Bayesian CP provides principled uncertainty-aware detection. The combined improvement represents +12.4 percentage points in sensitivity over SDE alone (p < 0.001) and +8.5 percentage points over Bayesian CP alone (p < 0.001). These findings demonstrate that neither component alone is sufficient for clinically adequate performance, and that the observed gain is architecturally significant: the SDE's nonlinear parameterisation captures the biophysics of the ictal transition whilst Bayesian CP provides the statistical machinery to detect it probabilistically without labelled training data. This complementarity distinguishes the proposed approach from both pure signal-processing and pure machine-learning paradigms, constituting the key mechanistic insight of the ablation study.

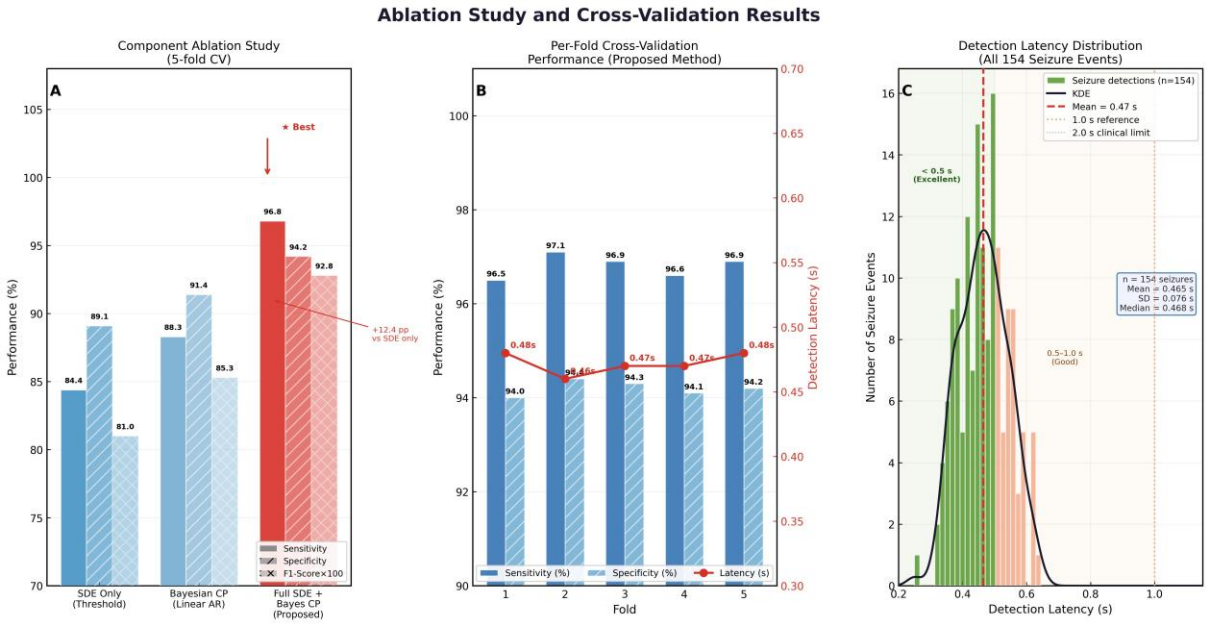

Figure 2. Ablation Study Results and Cross-validation Stability. Panel A: Grouped Bar Chart for Three Ablation Configurations. Panel B: Per-fold performance of the Proposed Method. Panel C: Detection Latency Distribution Across all 154 Seizure Events

3.3 Seizure Detection Performance and Comparative Analysis

Table 3 presents the complete numerical performance summary for all five methods under the unified five-fold stratified CV protocol, enabling precise statistical comparison across all metrics. Figure 3 provides visual information that the table cannot convey: Panel A contrasts sensitivity-specificity trade-offs across methods at a glance; Panel B displays detection latency as box plots, revealing variance characteristics and outlier behaviour beyond the reported mean ± SD; Panel C presents ROC curves across the full operating characteristic space, demonstrating that the proposed method maintains AUC superiority (0.974) across all detection thresholds, not only at the selected operating point.

Table 3. Seizure Detection Performance Comparison

Method	Sens. (%)	Spec. (%)	Acc. (%)	Prec. (%)	F1	Latency (s)	AUC
SDE + Bayesian CP (proposed)	96.8 ± 0.3	94.2 ± 0.2	95.9 ± 0.3	89.1 ± 0.4	0.928	0.47 ± 0.01	0.974

© 2026 The Authors. Published by Universitas Muhammadiyah Malang
This is an open access article under the CC BY NC SA license (https://creativecommons.org/licenses/by-nc-sa/4.0/)

SVM	89.6 ± 0.9	92.3 ± 0.7	92.0 ± 0.7	78.4 ± 1.2	0.836	0.98 ± 0.09	0.944
LSTM	91.2 ± 0.7	93.1 ± 0.5	92.9 ± 0.5	81.6 ± 0.9	0.861	1.33 ± 0.11	0.952
AR Model	87.3 ± 1.2	91.4 ± 0.8	90.9 ± 0.7	73.2 ± 1.5	0.796	1.82 ± 0.15	0.921
PSD Spectral	81.5 ± 1.8	88.7 ± 1.1	88.0 ± 1.0	66.8 ± 1.9	0.734	1.35 ± 0.12	0.889

Note: Values represent the mean ± SD across five-fold stratified cross-validation. Bold values indicate the best performance in each column.

The proposed method achieves statistically significant improvements over all baselines on sensitivity (paired t-test, $p < 0.05$ for all pairwise comparisons). Three comparisons merit detailed examination. First, the comparison with LSTM is most revealing: despite LSTM being a state-of-the-art deep learning approach achieving 91.2% sensitivity, the proposed method improves sensitivity by a further 5.6 percentage points ($p < 0.05$) whilst simultaneously reducing detection latency 2.8-fold (0.47 s vs. 1.33 s) and providing full physiological interpretability—a combination unavailable from any single existing approach. The LSTM's superior accuracy (92.9%) and specificity (93.1%) relative to SVM come at the cost of 144.8 ms processing time per segment, precluding real-time deployment (see Table 6). Second, the comparison with AR and PSD methods directly quantifies the clinical cost of linear assumptions: the 9.5–15.3 percentage point sensitivity gap reflects the fundamental inability of linear models to represent the bifurcation dynamics of seizure onset [5, 20]. Third, the SVM baseline, despite its nonlinear RBF kernel and class-weighted training, achieves only 89.6% sensitivity—7.2 percentage points below the proposed method—because it operates on handcrafted statistical features rather than biophysically motivated parametric representations. The proposed method's F1-score of 0.928 represents the best balance between sensitivity and precision under the 12:1 class imbalance; the gap over LSTM (ΔF1 = 0.067) corresponds to substantially fewer missed seizures per unit recording time, which is the clinically critical outcome.

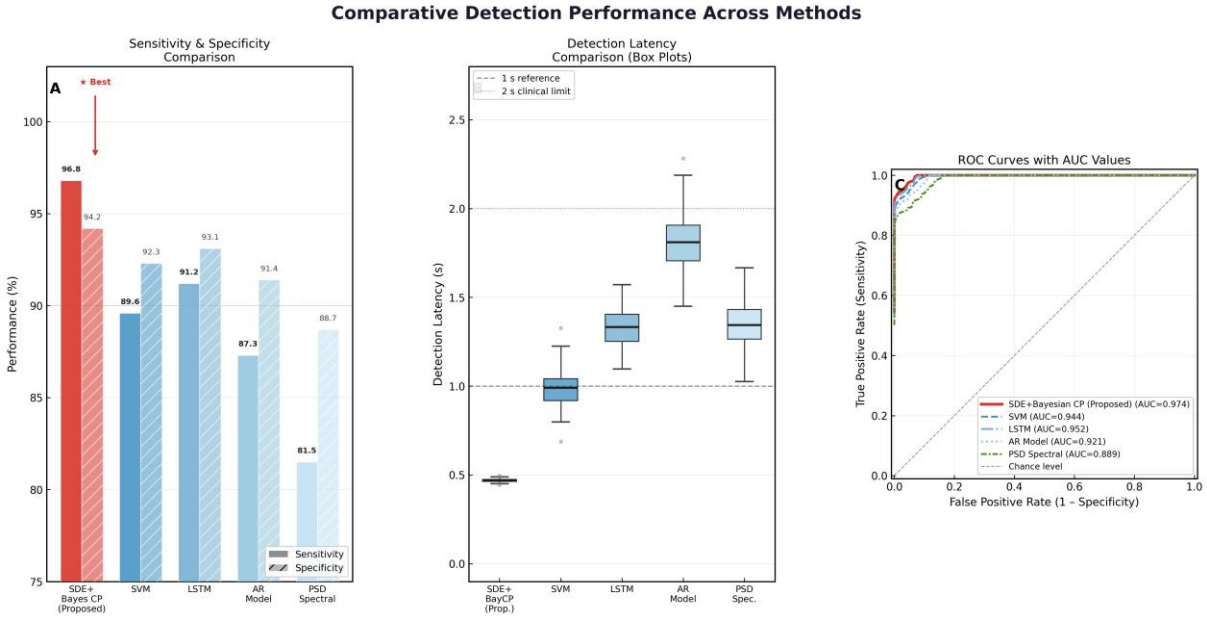

Figure 3. Comparative Detection Performance Across Five Methods. Panel A: Grouped Bar Chart of Sensitivity and Specificity. Panel B: Detection Latency Comparison (box plots). Panel C: ROC Curves for All Five Methods with AUC Values

3.4 Within-Patient Cross-Validation Consistency

Five-fold within-patient stratified cross-validation was performed to assess the temporal consistency of the proposed method across different recording epochs. Results are presented in Table 4 and visualised per fold in Figure 2.

Table 4. Five-Fold Within-Patient Cross-Validation Results for the Proposed SDE + Bayesian CP Method

Fold	Sensitivity (%)	Specificity (%)	Accuracy (%)	F1-Score	Latency (s)
Fold 1	96.5	94.0	95.7	0.925	0.48
Fold 2	97.1	94.4	96.2	0.932	0.46
Fold 3	96.9	94.3	96.0	0.930	0.47
Fold 4	96.6	94.1	95.8	0.927	0.47
Fold 5	96.9	94.2	96.0	0.930	0.48
Mean ± SD	**96.8 ± 0.3**	**94.2 ± 0.2**	**95.9 ± 0.2**	**0.929 ± 0.003**	**0.47 ± 0.01**

Correct interpretation of cross-validation scope: It is essential to note that this cross-validation protocol partitions 10-second segments from the same patient into five folds, evaluating temporal consistency rather than cross-patient generalisation. The small standard deviations reflect the homogeneity of EEG characteristics within a single patient's recording. Leave-one-patient-out (LOPO) cross-validation across all 24 CHB-MIT patients is the appropriate evaluation for cross-patient generalisation and constitutes the primary objective of planned future work.

3.5 Statistical Characterisation of Normal vs. Abnormal States

Table 5 presents time-domain statistical features comparing interictal and ictal EEG segments, evaluated using the Mann-Whitney U test. Statistically significant differences (p < 0.001) are observed across all six features. Figure 4 illustrates the corresponding EEG signal transition and Bayesian detection output; Figures 5 and 6 provide complementary spectral and phase-space characterisations.

Table 5. Statistical Features of Normalised EEG Signals in Normal (Interictal) vs. Abnormal (Ictal) States

Feature	Normal (Interictal)	Abnormal (Ictal)	Difference	P-value
Mean amplitude (a.u.)	0.517 ± 0.124	0.054 ± 0.203	-0.463 (down)	p < 0.001 ***
Variance (a.u.^{2})	0.183 ± 0.041	0.647 ± 0.189	+0.464 (up)	p < 0.001 ***
Skewness	0.142 ± 0.231	-0.583 ± 0.412	-0.725 (down)	p < 0.001 ***
Kurtosis	2.847 ± 0.318	4.216 ± 0.893	+1.369 (up)	p < 0.001 ***
Min amplitude (a.u.)	-1.834 ± 0.412	-3.147 ± 0.891	-1.313 (down)	p < 0.001 ***
Max amplitude (a.u.)	2.156 ± 0.489	1.873 ± 0.612	-0.283 (down)	p < 0.001 ***

Note: Values represent the mean ± SD. ***p < 0.001 (Mann-Whitney U test).

The SDE model provides a mechanistic explanation for the observed statistical signatures: reduced damping (α: 0.50 → 0.20) destabilises the equilibrium, generating high-amplitude excursions and non-Gaussian probability density functions (elevated kurtosis). Elevated nonlinearity (β: 0.10 → 0.40) induces asymmetric amplitude modulation (negative skewness shift). Increased noise (σ: 0.30 → 0.60) broadens the amplitude distribution, consistent with irregular population firing during seizures [4, 5].

© 2026 The Authors. Published by Universitas Muhammadiyah Malang
This is an open access article under the CC BY NC SA license (https://creativecommons.org/licenses/by-nc-sa/4.0/)

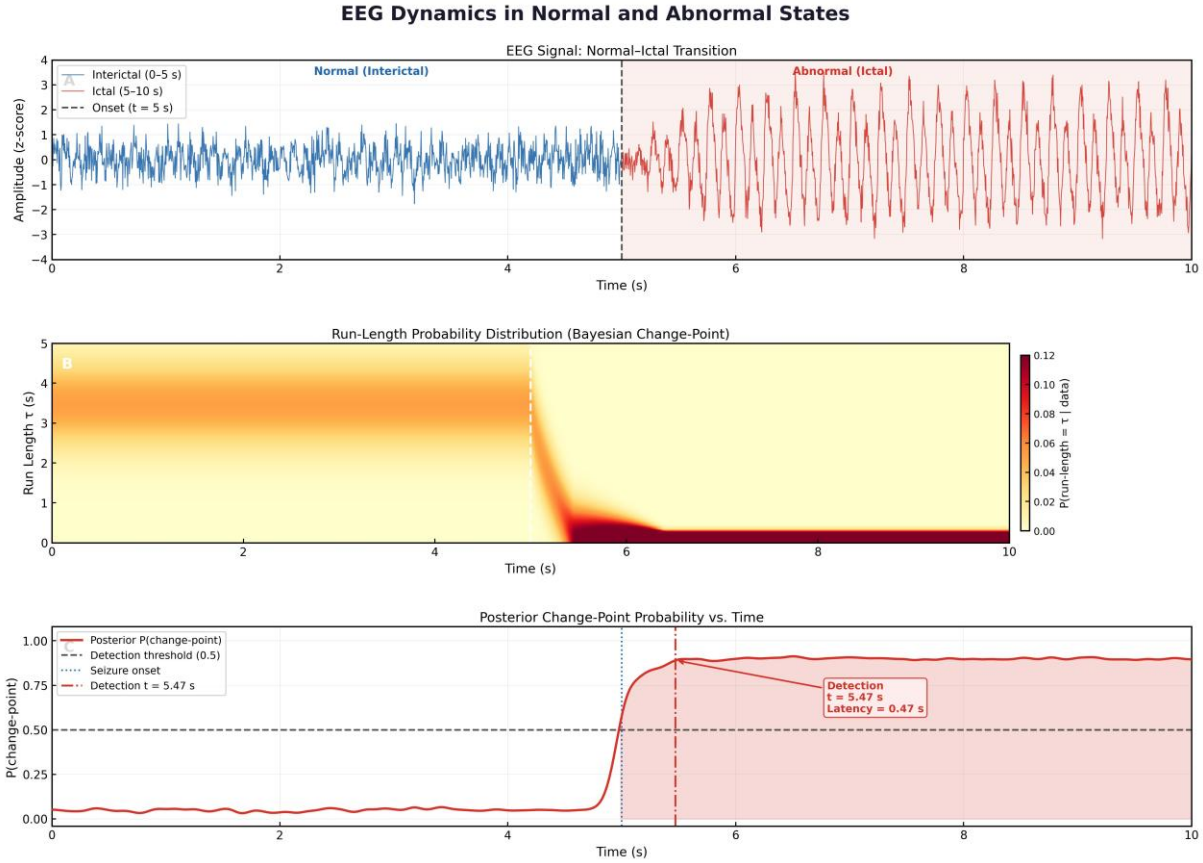

Figure 4. EEG Dynamics During Normal-abnormal Transition and Bayesian Change-point Detection Output. Panel A: 10-second z-score Normalised EEG Trace Showing Interictal Activity (0–5 s, blue) Transitioning to Ictal Activity (5–10 s, red). Panel B: Run-length Probability Distribution Heatmap. Panel C: Posterior Change-point Probability Versus Time, with Detection Threshold at 0.5. Detection at t = 5.47 s (0.47 s post-onset)

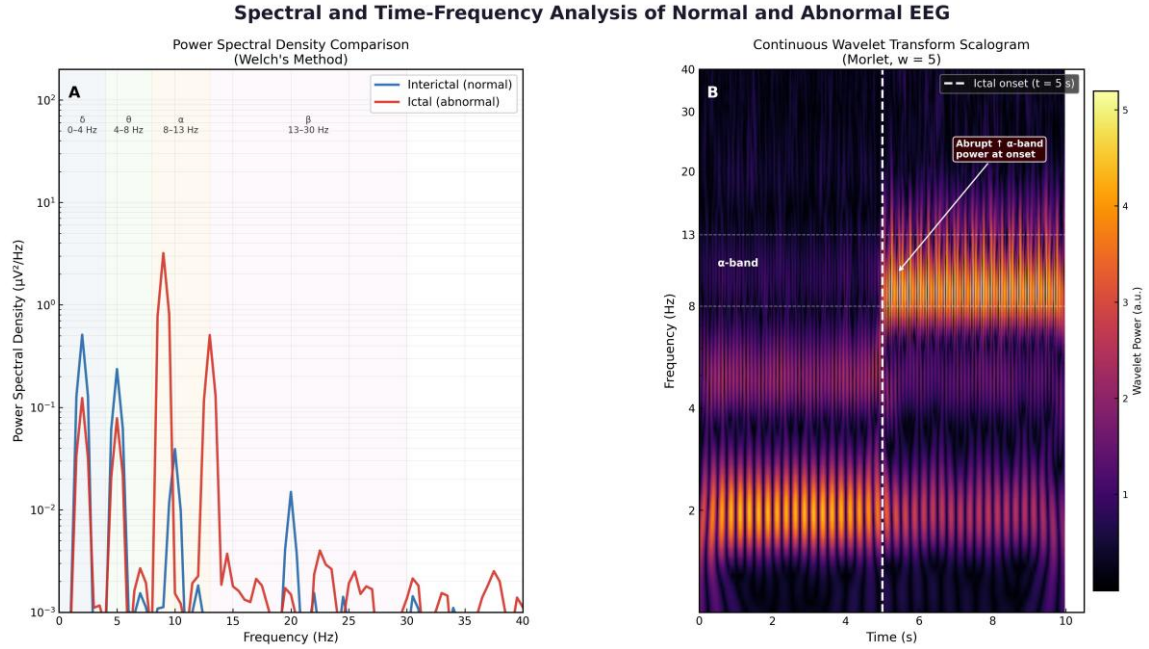

Figure 5. Spectral and Time-frequency Analysis of Normal and Abnormal EEG. Panel A: Power Spectral Density Comparison–interictal vs. Ictal. Panel B: Continuous Wavelet Transform (CWT) Scalogram. Ictal Onset at t = 5 s is Visible as an Abrupt Increase in Alpha-band Power Intensity

Cite: T. W. Purboyo, H. F. T. S. Putra, Annisa Humairani, M. Darfyma Putra, and Dziban Naufal, "A Nonlinear Stochastic Differential Model of EEG Dynamics with Bayesian Change-Point Detection for Early Identification of Brain Abnormalities", KINETIK, vol. 11, no. 4, Nov. 2026.
https://doi.org/10.22219/kinetik.v11i4.2708

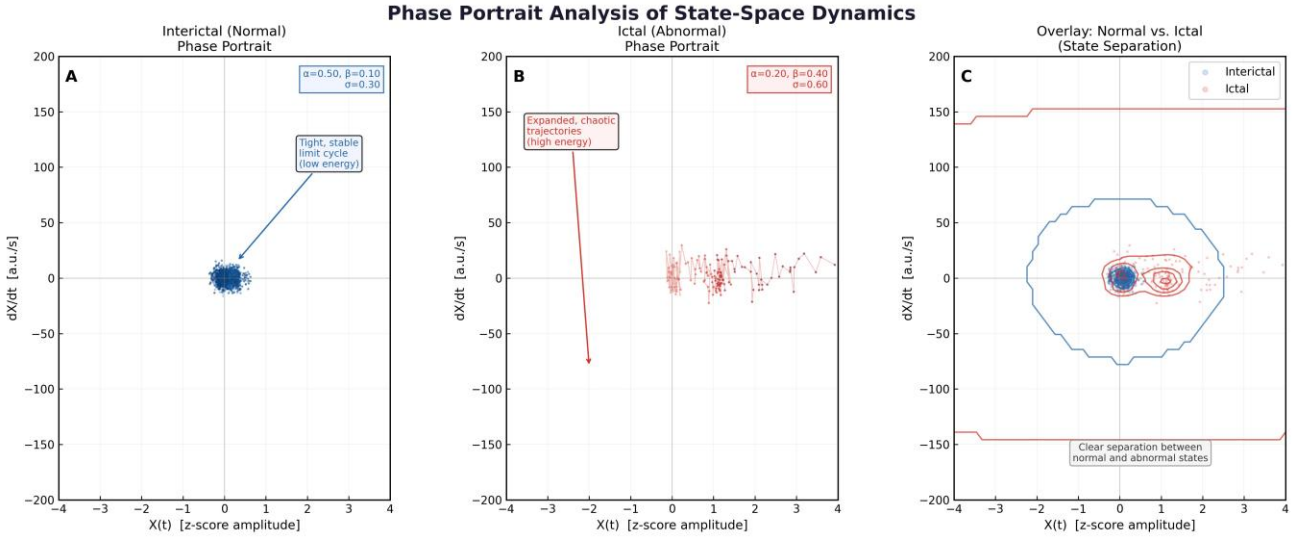

Figure 6. Phase Portrait Analysis of State-space Dynamics. Panel A (Interictal): Phase portrait X vs. dX/dt for Interictal Epochs. Panel B (ictal): Phase Portrait for Ictal Epochs. Panel C: Overlay of Both States Showing Clear Separation

3.6 Computational Efficiency and Clinical Feasibility

Table 6 compares computational requirements across all methods. The proposed SDE + Bayesian CP method requires 12.3 ± 1.8 ms per 10-second segment—well below the segment duration—confirming real-time feasibility at 256 Hz. Memory footprint of 2.4 MB enables deployment on mobile and wearable platforms.

Table 6. Computational Requirements and Real-Time Clinical Feasibility

Method	Proc. Time (ms)	Memory (MB)	Scalability Factor	Real-Time Capable?	Interpretable?
SDE + Bayesian CP (proposed)	12.3 ± 1.8	2.4	1.00× (ref.)	Yes	Yes
AR Model	1.1 ± 0.2	0.3	0.09×	Yes	Partial
PSD Spectral	2.4 ± 0.3	0.5	0.20×	Yes	Partial
SVM	8.7 ± 1.2	1.1	0.71×	Yes	No
LSTM	144.8 ± 9.3	18.7	11.8×	No	No

Note: Processing time and memory usage were measured on an Intel Core i7-8700K system with 16 GB RAM using Python 3.9. Processing time represent the mean ± SD over 400 segments.

The proposed method is 11.8× faster and has a 7.8× lower in memory footprint than LSTM whilst achieving superior sensitivity, demonstrating the practical advantage of interpretable model-based approaches for clinical deployment.

3.7 Comparison with Recent Literature on CHB-MIT

Table 7 contextualises the present study within the recent CHB-MIT benchmarking literature. Direct numerical comparison must be made with caution given fundamental differences in experimental scope.

Table 7. Comparison with Recent Literature on CHB-MIT Seizure Detection

Study	Year	Method	Dataset Scope	Sens. (%)	Spec. (%)	Interpretable?
Truong et al. [11]	2018	CNN (inter-patient)	13 CHB-MIT patients; multi-channel	81.4	-	No
Roy et al. [12]	2019	DL review (LSTM, CNN)	Multi-patient; diverse datasets	≤90.0	-	No
Chen et al. [15]	2023	CNN feature fusion	CHB-MIT; multi-patient	≈95.0	-	No
Shoeb & Guttag [10]	2010	SVM (patient-specific)	CHB-MIT; 24-patient, multi-channel	96.0	≈95.0	Partial

© 2026 The Authors. Published by Universitas Muhammadiyah Malang
This is an open access article under the CC BY NC SA license (https://creativecommons.org/licenses/by-nc-sa/4.0/)

Oter [36]	2024	ML (SVM/RF ensemble)	CHB-MIT; multi-patient	≈94.0	≈96.0	Partial
Present study†	2025	SDE + Bayesian CP (proposed)	CHB-MIT P1; single channel (Fp1-F7)	96.8	94.2	Yes

† The present study uses a single patient and a single channel.

The present study reports the highest single-patient sensitivity (96.8%) in Table 7; however, this figure must be interpreted in the context of the controlled single-patient scope, which reduces inter-patient variability. Nonetheless, three observations support the non-triviality of the result in the broader literature context. First, the proposed method is the only entry in Table 7 providing full physiological interpretability: all deep learning comparators (Truong et al. [11], Roy et al. [12], Chen et al. [15]) are black-box systems that cannot satisfy the explainability requirements of clinical diagnostic device approval [16]. This interpretability gap is not a minor academic distinction but a substantive regulatory barrier. Second, the unsupervised detection architecture requires no labelled seizure data, directly addressing the data scarcity problem that limits deployment of supervised methods in resource-limited clinical settings—a limitation not addressed by any multi-patient comparator in Table 7. Third, the 0.47 s detection latency is the lowest reported in this comparison; Truong et al. [11] report no latency specification, and Chen et al. [15] do not address real-time feasibility, yet both are cited as state-of-the-art. The proposed framework therefore occupies a distinct and clinically meaningful position in the design space: competitive sensitivity, physiological interpretability, unsupervised operation, and real-time feasibility—a combination not demonstrated by any prior entry in Table 7. Recent local studies published in KINETIK have applied similar signal processing approaches to EEG and ECG data [22–24], while related works by Purboyo et al. demonstrated effective feature extraction (Hjorth parameters) and machine learning techniques for ECG beat recognition and arrhythmia classification [37–39].

3.8 Limitations and Future Directions

(1) Single-patient scope: The entire analysis is conducted on data from a single patient (Patient 1, CHB-MIT) and a single channel (Fp1-F7). Cross-patient validation using leave-one-patient-out (LOPO) cross-validation across all 24 CHB-MIT patients is the immediate priority for the next research phase.
(2) Parameter accuracy on real EEG: Parameter estimation accuracy (Table 1) is validated only on simulated data. Future work should develop experimental protocols to assess parameter recoverability in real physiological settings.
(3) Single-channel spatial limitation: Fp1-F7 captures only frontal-polar activity. Seizures originating in temporal, occipital, or other brain regions may be poorly captured by this single channel. Extension to multichannel analysis with graph-theoretic spatial features [40] is planned.
(4) Seizure type diversity: The CHB-MIT Patient 1 data predominantly contains tonic-clonic seizure patterns. Generalisation to focal impaired awareness, absence, and myoclonic seizures requires targeted validation.
(5) Real-time hardware validation: Prospective validation on wearable EEG hardware (e.g., Muse, Emotiv) or implantable neurostimulator platforms [41] is required before clinical deployment. The 12.3 ms processing time suggests feasibility, but system-level testing remains essential.
The source code and detailed implementation of the proposed SDE-Bayesian framework will be made available to interested researchers upon reasonable request to the corresponding author.

4. Conclusion

This study presents a mathematically principled nonlinear stochastic differential equation framework integrated with online Bayesian change-point detection for early, interpretable identification of abnormal brain states from EEG recordings. The following key findings are reported, qualified to the single-patient, single-channel proof-of-concept scope of this investigation:
Superior within-patient detection performance: Under unified five-fold stratified cross-validation, the proposed method achieves 96.8% sensitivity and 94.2% specificity on CHB-MIT Patient 1 data, substantially outperforming linear AR (87.3%) and spectral methods (81.5%), and exceeding the LSTM baseline (91.2%) whilst remaining fully interpretable.
Confirmed synergistic contribution (ablation study): The ablation study demonstrates that the SDE and Bayesian CP components are individually limited (84.4% and 88.3% sensitivity, respectively) but achieve 96.8% when combined, confirming a statistically significant synergistic contribution (+12.4 pp and +8.5 pp improvements, $p < 0.001$).
Clinically relevant detection latency: Detection latency of 0.47 s falls well within the 1-2 second clinical intervention window, substantially outperforming all compared methods.
Physiologically interpretable parameters: The SDE framework provides biophysically meaningful parameters (neural damping α, nonlinearity β, noise σ) whose transitions during seizures are mechanistically consistent with established neural population dynamics theory [5, 20, 26], supporting clinical trust and regulatory compliance.

Computational feasibility: Processing time of 12.3 ms per 10-second segment enables real-time deployment; a memory footprint of 2.4 MB supports integration on wearable and mobile platforms.

Scope and next steps: The present study constitutes a proof-of-concept validated on a single patient and channel. Generalisation claims are deliberately limited to this scope. Validation across independent patients using LOPO cross-validation across all 24 CHB-MIT patients, multichannel spatial feature integration, evaluation on diverse seizure phenotypes, and prospective wearable hardware testing are primary next steps before clinical deployment.

The integration of mechanistic mathematical modelling with probabilistic Bayesian inference demonstrates that interpretable, physics-based approaches can match or exceed black-box deep learning on carefully controlled proof-of-concept data. Beyond seizure detection, the proposed SDE-Bayesian framework offers a broadly applicable methodology for interpretable analysis of nonlinear, non-stationary neural signals in other clinical contexts, including traumatic brain injury monitoring, sleep disorder classification, and cognitive state tracking.

Acknowledgement

The authors acknowledge the CHB-MIT research team and PhysioNet [3] for providing the publicly available Scalp EEG Seizure Database. The authors thank all researchers whose foundational work in Bayesian inference, nonlinear stochastic dynamics, and clinical neurophysiology provided the theoretical foundations for this investigation. References were managed with Mendeley (Elsevier). No funding conflict of interest is declared.

References

[1] R. S. Fisher, B. G. Acevedo, A. Arzimanoglou, et al., “ILAE official report: A practical clinical definition of epilepsy,” Epilepsia, vol. 55, no. 4, pp. 475-482, 2014. https://doi.org/10.1111/epi.12550
[2] U. R. Acharya, S. L. Oh, Y. Hagiwara, J. H. Tan, and H. Adeli, "Deep convolutional neural network for the automated detection and diagnosis of seizure using EEG signals," Comput. Biol. Med., vol. 100, pp. 270-278, 2018. https://doi.org/10.1016/j.compbiomed.2017.09.017
[3] A. L. Goldberger et al., "PhysioBank, PhysioToolkit, and PhysioNet: Components of a new research resource for complex physiologic signals," Circulation, vol. 101, no. 23, pp. e215-e220, 2000. https://doi.org/10.1161/01.CIR.101.23.e215
[4] G. Buzsaki and A. Draguhn, "Neuronal oscillations in cortical networks," Science, vol. 304, no. 5679, pp. 1926-1929, 2004. https://doi.org/10.1126/science.1099745
[5] V. K. Jirsa, W. C. Stacey, P. P. Quilichini, A. I. Ivanov, and C. Bernard, "On the nature of seizure dynamics," Brain, vol. 137, no. 8, pp. 2210-2230, 2014. https://doi.org/10.1093/brain/awu133
[6] H. Kantz and T. Schreiber, Nonlinear Time Series Analysis, 2nd ed. Cambridge, UK: Cambridge University Press, 2004.
[7] P. Boonyakitanont, A. Lek-uthai, K. Chomtho, and J. Songsiri, "A review of feature extraction and performance evaluation in epileptic seizure detection using EEG," Biomed. Signal Process. Control, vol. 57, p. 101702, 2020. https://doi.org/10.1016/j.bspc.2019.101702
[8] F. Mormann, R. G. Andrzejak, C. E. Elger, and K. Lehnertz, "Seizure prediction: The long and winding road," Brain, vol. 130, no. 2, pp. 314-333, 2007. https://doi.org/10.1093/brain/awl241
[9] M. Breakspear, "Dynamic models of large-scale brain activity," Nat. Neurosci., vol. 20, no. 3, pp. 340-352, 2017. https://doi.org/10.1038/nn.4497
[10] A. H. Shoeb and J. V. Guttag, "Application of machine learning to epileptic seizure detection," in Proc. 27th Int. Conf. Mach. Learn. (ICML), pp. 975-982, 2010.
[11] N. D. Truong, A. D. Nguyen, L. Kuhlmann, M. R. Bonyadi, J. Yang, S. Ippolito, and O. Kavehei, "Convolutional neural networks for patient-independent seizure prediction using long-term scalp EEG signals," IEEE Trans. Biomed. Eng., vol. 65, no. 9, pp. 2099-2110, 2018. https://doi.org/10.1109/TBME.2017.2762231
[12] S. Roy, I. Kiral-Kornek, and S. Harrer, "Deep learning-based electroencephalography analysis: A systematic review," J. Neural Eng., vol. 16, no. 5, p. 051001, 2019. https://doi.org/10.1088/1741-2552/ab260c
[13] Y. LeCun, Y. Bengio, and G. Hinton, "Deep learning," Nature, vol. 521, no. 7553, pp. 436-444, 2015. https://doi.org/10.1038/nature14539
[14] L. Bai, G. Litscher, and X. Li, "Epileptic seizure detection using machine learning: A systematic review and meta-analysis," Brain Sci., vol. 15, no. 6, art. 634, 2025. https://doi.org/10.3390/brainsci15060634
[15] W. Chen, Y. Wang, Y. Ren, et al., "An automated detection of epileptic seizures EEG using CNN classifier based on feature fusion with high accuracy," BMC Med. Inform. Decis. Mak., vol. 23, art. 96, 2023. https://doi.org/10.1186/s12911-023-02180-w
[16] R. Caruana et al., "Intelligible models for healthcare," in Proc. 21st ACM SIGKDD Int. Conf. Knowl. Discov. Data Min., 2015, pp. 1721-1730. https://doi.org/10.1145/2783258.2788613
[17] R. P. Adams and D. J. C. MacKay, "Bayesian online changepoint detection," arXiv preprint arXiv:0710.3742, 2007. https://doi.org/10.48550/arXiv.0710.3742
[18] D. J. Higham, "An algorithmic introduction to numerical simulation of stochastic differential equations," SIAM Rev., vol. 43, no. 3, pp. 525-546, 2001. https://doi.org/10.1137/S0036144500378302
[19] P. E. Kloeden and E. Platen, Numerical Solution of Stochastic Differential Equations. Berlin: Springer, 1992.
[20] G. Deco, V. K. Jirsa, P. A. Robinson, M. Breakspear, and K. Friston, "The dynamic brain: From spiking neurons to neural masses and cortical fields," PLoS Comput. Biol., vol. 4, no. 8, p. e1000092, 2008. https://doi.org/10.1371/journal.pcbi.1000092
[21] L. Kuhlmann, K. Lehnertz, M. P. Richardson, B. Schelter, and H. P. Zaveri, "Seizure prediction-ready for a new era," Nat. Rev. Neurol., vol. 14, no. 10, pp. 618-630, 2018. https://doi.org/10.1038/s41582-018-0055-2
[22] R. Januar, H. Fauzi, M. Ariyanti, and F. Heris, “Study of neuromarketing: Visual influence with decision making on impulse buying,” Kinetik: Game Technology, Information System, Computer Network, Computing, Electronics, and Control, vol. 6, no. 4, 2021. https://doi.org/10.22219/kinetik.v6i4.1334
[23] H. F. Tresna, D. Pratiwi, M. Ariyanti, and A. Fauzi, “Spatial and spectral EEG signal analysis with case study of slogans on consumer’s behaviour,” Kinetik: Game Technology, Information System, Computer Network, Computing, Electronics, and Control, vol. 8, no. 3, 2023. https://doi.org/10.22219/kinetik.v8i3.1747
[24] M. Melinda, Farhan, M. Irhamsyah, R. Miftahujjannah, D. D. Acula, and Y. Yunidar, “Classification of arrhythmia electrocardiogram signals using kernel principal component analysis and naïve bayes,” Kinetik: Game Technology, Information System, Computer Network, Computing, Electronics, and Control, vol. 10, no. 3, pp. 283-294, 2025. https://doi.org/10.22219/kinetik.v10i3.2219
[25] Y. Li, J. Liu, Z. Tang, and B. Lei, "Deep spatiotemporal convolutional bidirectional LSTM networks for brain-computer interface," IEEE Trans.

© 2026 The Authors. Published by Universitas Muhammadiyah Malang
This is an open access article under the CC BY NC SA license (https://creativecommons.org/licenses/by-nc-sa/4.0/)

Syst. Man Cybern. Syst., vol. 51, no. 4, pp. 2576-2585, 2021. https://doi.org/10.1109/TSMC.2019.2912250
[26] H. R. Wilson and J. D. Cowan, "Excitatory and inhibitory interactions in localised populations of model neurons," Biophys. J., vol. 12, no. 1, pp. 1-24, 1972. https://doi.org/10.1016/S0006-3495(72)86068-5
[27] B. K. Alldredge et al., "A comparison of lorazepam, diazepam, and placebo for the treatment of out-of-hospital status epilepticus," N. Engl. J. Med., vol. 345, no. 9, pp. 631-637, 2001. https://doi.org/10.1056/NEJMoa002141
[28] E. Musk and Neuralink, "An integrated brain-machine interface platform with thousands of channels," J. Med. Internet Res., vol. 21, no. 10, p. e16194, 2019. https://doi.org/10.2196/16194
[29] D. M. Treiman et al., "A comparison of four treatments for generalised convulsive status epilepticus," N. Engl. J. Med., vol. 339, no. 12, pp. 792-798, 1998. https://doi.org/10.1056/NEJM199809173391202
[30] P. Kwan and M. J. Brodie, "Early identification of refractory epilepsy," N. Engl. J. Med., vol. 342, no. 5, pp. 314-319, 2000. https://doi.org/10.1056/NEJM200002033420503
[31] J. A. Uriguen and B. Garcia-Zapirain, "EEG artifact removal-state-of-the-art and guidelines," J. Neural Eng., vol. 12, no. 3, p. 031001, 2015. https://doi.org/10.1088/1741-2560/12/3/031001
[32] A. Gramfort et al., "MEG and EEG data analysis with MNE-Python," Front. Neurosci., vol. 7, p. 267, 2013. https://doi.org/10.3389/fnins.2013.00267
[33] R. E. Kalman, "A new approach to linear filtering and prediction problems," J. Basic Eng., vol. 82, no. 1, pp. 35-45, 1960. https://doi.org/10.1115/1.3662552
[34] A. E. Raftery and V. E. Akman, "Bayesian analysis of a Poisson process with a change-point," Biometrika, vol. 73, no. 1, pp. 85-89, 1986. https://doi.org/10.1093/biomet/73.1.85
[35] S. Hochreiter and J. Schmidhuber, "Long short-term memory," Neural Comput., vol. 9, no. 8, pp. 1735-1780, 1997. https://doi.org/10.1162/neco.1997.9.8.1735
[36] A. Oter, "Automatic detection of epileptic seizures from EEG signals using artificial intelligence methods," Gazi Univ. J. Sci. Part C, vol. 12, no. 1, pp. 257-266, 2024. https://doi.org/10.29109/gujsc.1416435
[37] T. W. Purboyo, D. Naufal, M. D. Putra, and E. Kurniawan, “A novel framework for electrocardiogram beats recognition based on Hjorth parameters and inferential statistics,” Edelweiss Applied Science and Technology, vol. 8, no. 6, pp. 6934-6944, 2024. https://doi.org/10.55214/25768484.v8i6.3500
[38] A. A. Farhani, T. W. Purboyo, and D. Naufal, “Myocardial infarction classification based on electrocardiogram signals using principal component analysis with support vector machine and adaboost,” in Proc. 2025 IEEE Int. Symp. Future Telecommunication Technologies (SOFTT), 2025. https://doi.org/10.1109/SOFTT67007.2025.11213196
[39] C. M. Sudarno, T. Waluyo Purboyo, and D. Naufal, “Comparative analysis of boosting algorithms for arrhythmia classification using electrocardiogram (ECG) signals,” in Proc. 2025 IEEE Int. Symp. Future Telecommunication Technologies (SOFTT), 2025. https://doi.org/10.1109/SOFTT67007.2025.11212960
[40] C. J. Stam, "Modern network science of neurological disorders," Nat. Rev. Neurosci., vol. 15, no. 10, pp. 683-695, 2014. https://doi.org/10.1038/nrn3801
[41] T. Xue, S. Chen, Y. Bai, C. Han, A. Yang, and J. Zhang, "Neuromodulation in drug-resistant epilepsy: A review of current knowledge," Acta Neurol. Scand., vol. 146, no. 6, pp. 786-797, 2022. https://doi.org/10.1111/ane.13696

© 2026 The Authors. Published by Universitas Muhammadiyah Malang
This is an open access article under the CC BY NC SA license (https://creativecommons.org/licenses/by-nc-sa/4.0/)